Supporting information

Unravelling the Impact of Buried Interface Voids on Hysteresis in Perovskite Solar Cells via Opto-Electro-Ionic Simulation

*Haoyang Wu[a], Zhihao Xu[a], Jiahui Chen[a], Juntao Wang[a], Yichu Zheng[a]**

[a] School of Mechatronic Engineering and Automation, Shanghai University, Shanghai 200444, China

*** Corresponding Author:** Yichu Zheng, Email: yczheng@shu.edu.cn

Supplementary Note S1.

In this study, the numerical simulations were performed. The corresponding electrical stimulation could be carried out by coupling Poisson's equation, drift-diffusion equations, and current continuity equations. Among them, Poisson's equation, which calculates the potential distribution, is given by

$$\frac{\partial^2\varphi(x)}{\partial^2 x^2} = -\frac{q}{\varepsilon_0\varepsilon_r}(p(x) - n(x) + N_D(x) - N_A(x)) \tag{S1}$$

where $\varphi(x)$ is a local electric potential, ε_0 is the permittivity of vacuum, ε_r is the relative permittivity, q is the elementary charge, $n(x)$ and $p(x)$ are the electron density and hole density. $N_D(x)$ and $N_A(x)$ are the donor and the acceptor densities. However, when the ionic migration behavior within the perovskite is taken into account, the influence of the change in ionic concentration on the local electric potential $\varphi(x)$ needs to be additionally considered. Therefore, the Poisson's equation needs to be transformed as follows

$$\frac{\partial^2\varphi(x)}{\partial^2 x^2} = -\frac{q}{\varepsilon_0\varepsilon_r}(p(x) - n(x) + c(x) - a(x) + N_D(x) - N_A(x)) \tag{S2}$$

where $c(x)$ and $a(x)$ are the cation density and anion density.

The entire perovskite satisfies the neutral condition through the following equation

$$1/wt \iint a(x)dx = 1/wt \iint c(x)dx = NI \tag{S3}$$

where w is the total width of perovskite, t is the total thickness of perovskite and NI is ion density.

The electric field distribution $F(x)$ is calculated from the relation

$$F(x) = \frac{\partial\varphi(x)}{\partial x} \tag{S4}$$

Based on the approximate and simplified Boltzmann statistical distribution, the current density of PSCs can be approximated using the drift-diffusion model, where the behavior of electrons and holes is quantitatively described by the following drift-diffusion equations

$$J_n(x) = q\mu_n n(x)\frac{\partial\varphi(x)}{\partial x} + qD_n\frac{\partial n(x)}{\partial x} \tag{S5}$$

$$J_p(x) = q\mu_p p(x)\frac{\partial\varphi(x)}{\partial x} + qD_p\frac{\partial p(x)}{\partial x} \tag{S6}$$

where the $J_n(J_p)$,$\mu_n(\mu_p)$,and $D_n(D_p)$ are the electron (hole) current densities, electron (hole) mobility, and electron (hole) diffusion coefficients, respectively.

Similar to electrons and holes, the current densities of anions and cations can also be approximated using the drift-diffusion equations

$$J_a(x) = q\mu_a a(x)\frac{\partial\varphi(x)}{\partial x} + qD_a\frac{\partial a(x)}{\partial x} \tag{S7}$$

$$J_c(x) = q\mu_c c(x)\frac{\partial\varphi(x)}{\partial x} + qD_c\frac{\partial c(x)}{\partial x} \tag{S8}$$

where the $J_a(J_c)$,$\mu_a(\mu_c)$,and $D_a(D_c)$ are the anion (cation) current densities, anion (cation) mobility, and anion (cation) diffusion coefficients, respectively.The diffusion constants could be obtained via Einstein relations as

$$D = \frac{\mu k_B T}{q} \tag{S9}$$

where k_B is the Boltzmann constant and T is the absolute temperature.

The continuous equations used in this work describe generation, recombination, and transport processes given by

$$\frac{\partial n(x)}{\partial t} = G_n(x) - R_n(x) + \frac{1}{q}\frac{\partial J_n(x)}{\partial x} \quad \text{(S10)}$$

$$\frac{\partial p(x)}{\partial t} = G_p(x) - R_p(x) - \frac{1}{q}\frac{\partial J_p(x)}{\partial x} \quad \text{(S11)}$$

where $G_n(x)$ and $G_p(x)$ are the generation rate for electrons and holes, $R_n(x)$ and $R_p(x)$ are recombination rates for electrons and holes.

The mobile ions within the perovskite also satisfy the continuous equations. Unlike electrons and holes, ions are not generated by light or recombination. Therefore, the continuous equations for anion and cation can be expressed as

$$\frac{\partial a(x)}{\partial t} = \frac{1}{q}\frac{\partial J_a(x)}{\partial x} \quad \text{(S12)}$$

$$\frac{\partial c(x)}{\partial t} = \frac{1}{q}\frac{\partial J_c(x)}{\partial x} \quad \text{(S13)}$$

The generation rate is given by

$$G(x) = \int_{\lambda_{min}}^{\lambda_{max}} \alpha(\lambda) N_{photo}(\lambda,x) d\lambda \quad \text{(S14)}$$

where λ is the wavelength and N_{photo} is the photon flux at each position, $\alpha(\lambda)$ is the wavelength-dependent absorptivity calculated from complex refractive index of material by

$$\alpha(\lambda) = \frac{4\pi k(\lambda)}{\lambda} \quad \text{(S15)}$$

where $k(\lambda)$ is the extinction coefficient.

The recombination rate in the continuity equations was obtained by employing different recombination models. Herein, direct recombination, Shockley-Read-Hall (SRH) recombination, and Auger recombination are considered as

$$R(x) = R_{Direct} + R_{SRH} + R_{Auger} \tag{S16}$$

The direct recombination model equation is given by

$$R_{Direct}(x) = C(n(x)p(x) - n_i^2(x)) \tag{S17}$$

where C and $n_i(x)$ are direct recombination coefficient and intrinsic carrier density, respectively.The n_i is given by

$$n_i^2(x) = N_C N_V exp(-\frac{E_g}{k_B T}) \tag{S18}$$

where E_g is the bandgap, N_C, N_V are the effective density of states (DOS).

The Auger recombination equation is given by

$$R_{Auger}(x) = (C_n n(x) + C_p p(x))(n(x)p(x) - n_i^2(x)) \tag{S19}$$

where C_n and C_p are electron and hole auger coefficient for electrons and holes, respectively.

The Shockley-Read-Hall (SRH) recombination equation is given by

$$R_{SRH}(x) = \frac{n(x)p(x) - n_i^2(x)}{\tau_n(p(x) + p_1(x)) + \tau_p(n(x) + n_1(x))} \tag{S20}$$

where τ_n and τ_p are the SRH lifetimes for electrons and holes, which could be obtained by

$$\tau_n = \frac{1}{N_t V_{th}^e \sigma_e} \tag{S21}$$

$$\tau_p = \frac{1}{N_t V_{th}^h \sigma_h} \tag{S22}$$

where $N_t$is the trap density, V_{th}^e and V_{th}^h are thermal velocity for electrons and holes, σ_e and σ_h are capture cross section for electrons and holes, respectively. The parameters $n_1(x)$ and $p_1(x)$ are given by

$$n_1(x) = N_C exp(- \frac{E_C - E_t}{k_B T}) \quad \text{(S23)}$$

$$p_1(x) = N_V exp(- \frac{E_t - E_V}{k_B T}) \quad \text{(S24)}$$

wheres E_C and E_V are the edge of conduction band and valance band, and E_t is the trap energy level that located in the middle of bandgap.

By solving these equations, the electrical parameters/properties including J-V characteristic curves and distributions of electric field, current density, recombination rate, etc., could be obtained by employing the key parameters listed in Table S1.

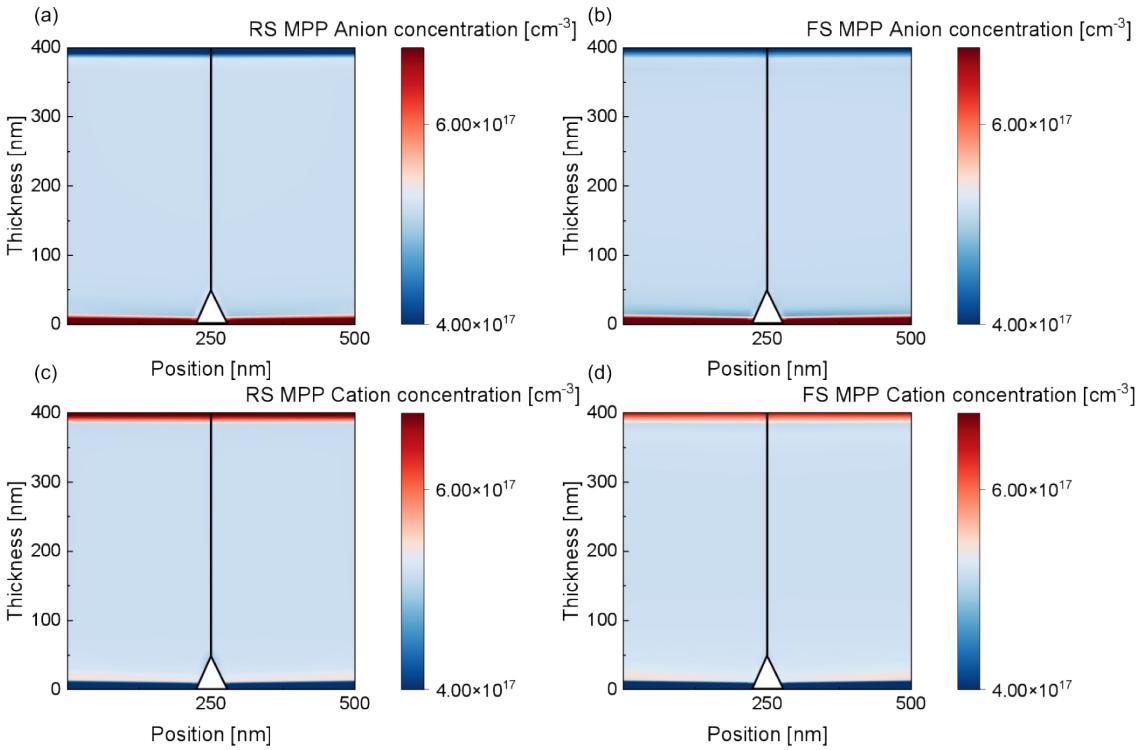

Supplementary Figure S1. The distribution of anion concentration under (a) reverse scanning and (b) forward scanning at MPP, and the distribution of cation concentration under (c) reverse scanning and (d) forward scanning at MPP.

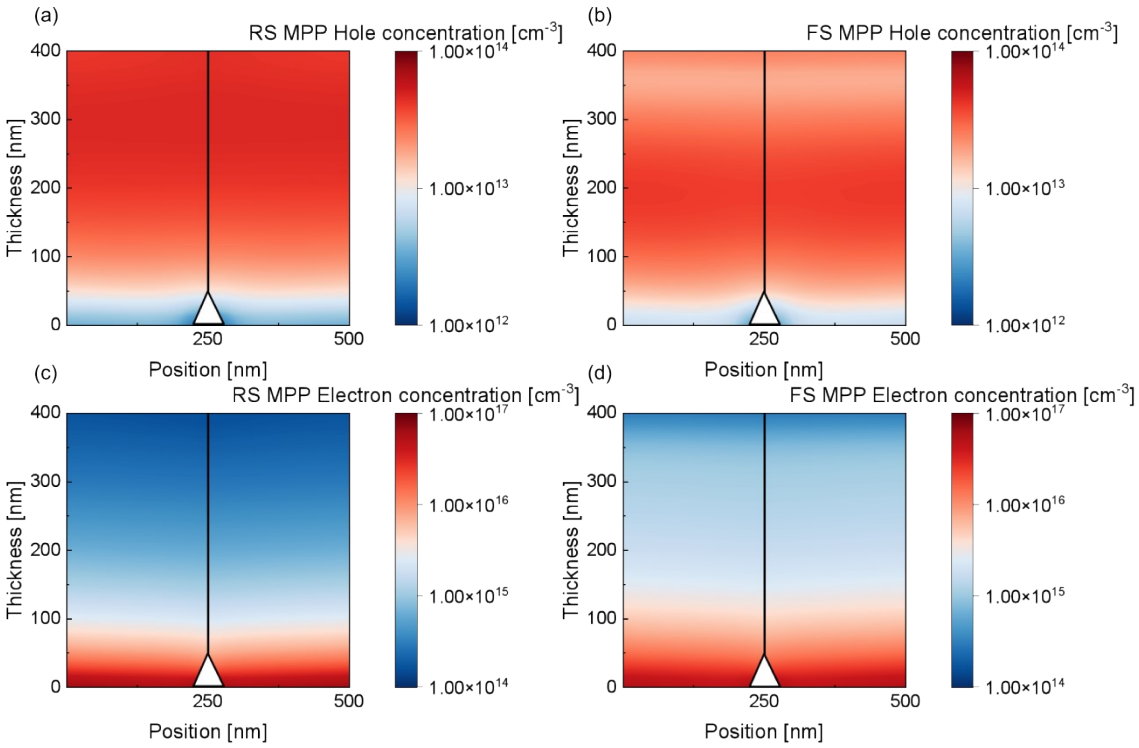

Supplementary Figure S2. The distribution of hole concentration under (a) reverse scanning and (b) forward scanning at MPP, and the distribution of electron concentration under (c) reverse scanning and (d) forward scanning at MPP.

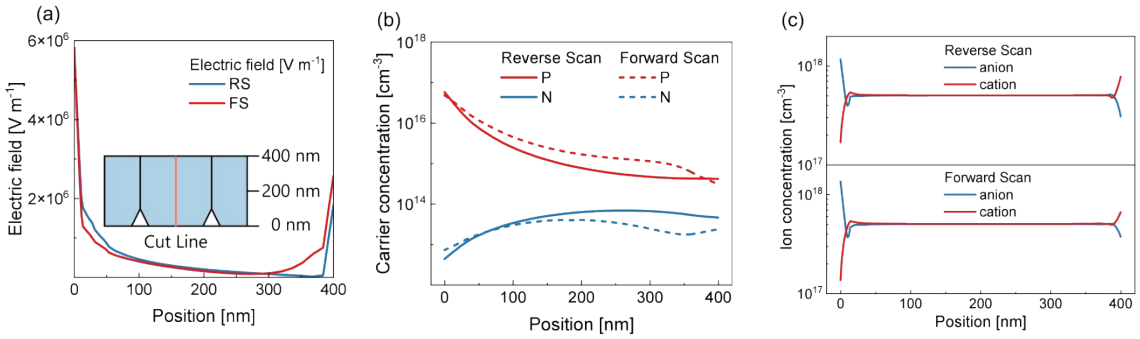

Supplementary Figure S3. (a) The distribution of electric field intensity along the cut line shown in the inset. (b) Carrier concentration and (c) ion concentration along the cut line for void devices.

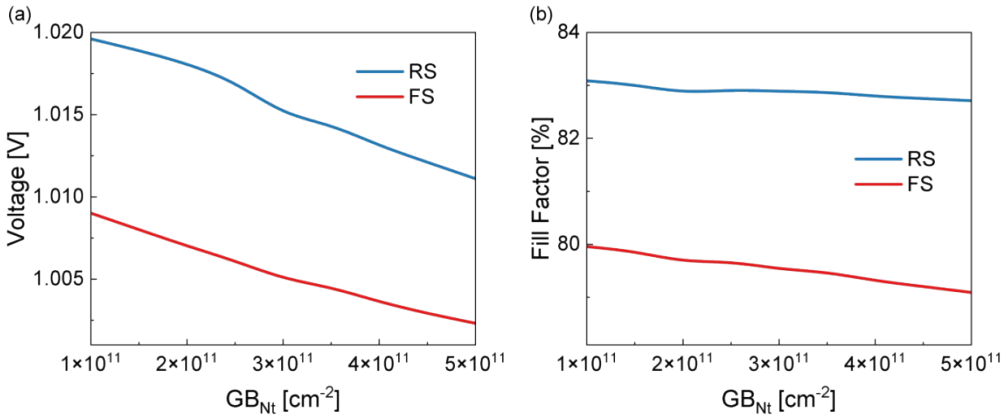

Supplementary Figure S4. (a) Voc and (b) FF of void devices with GB at various defect density.

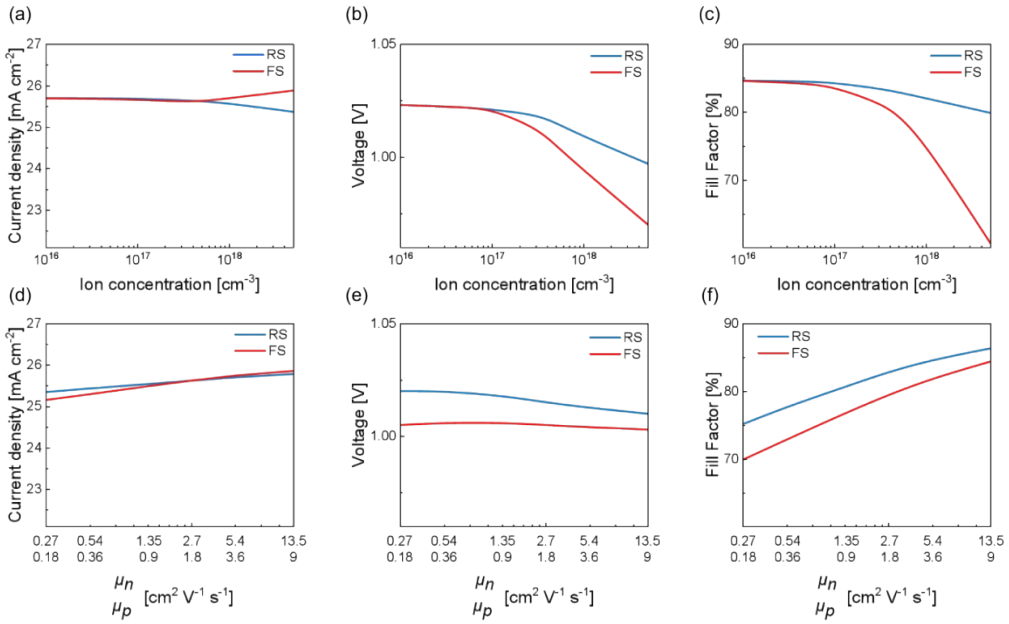

Supplementary Figure S5. Jsc (a) , Voc (b) and FF (c) of PSCs at various ion concentrations. Jsc (d) , Voc (e) and FF (f) of PSCs at various carrier mobilities.

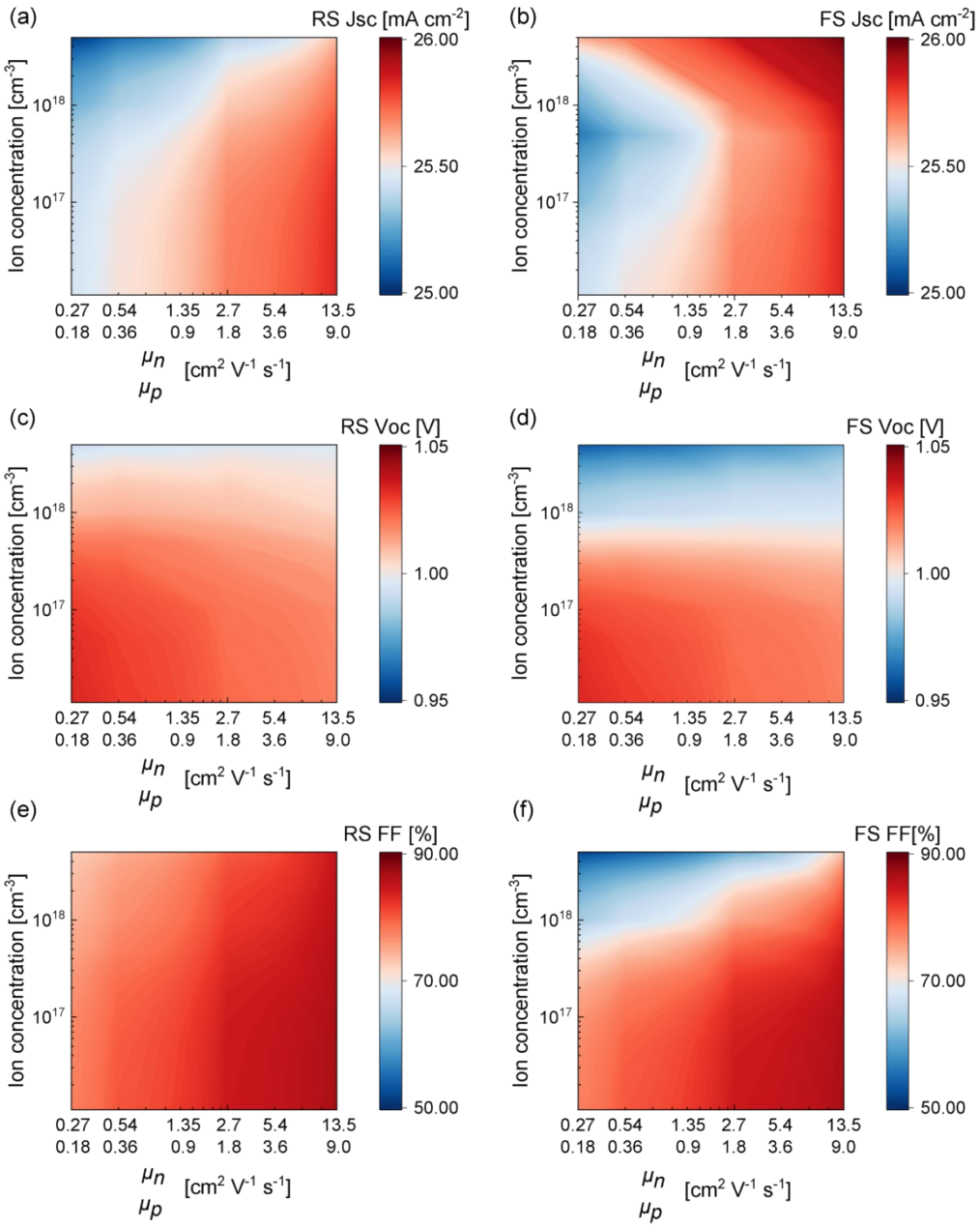

Supplementary Figure S6. (a-b) Jsc , (c-d) Voc and (e-f) FF contour maps under forward and reverse voltage scans with various carrier mobility and ion concentration .

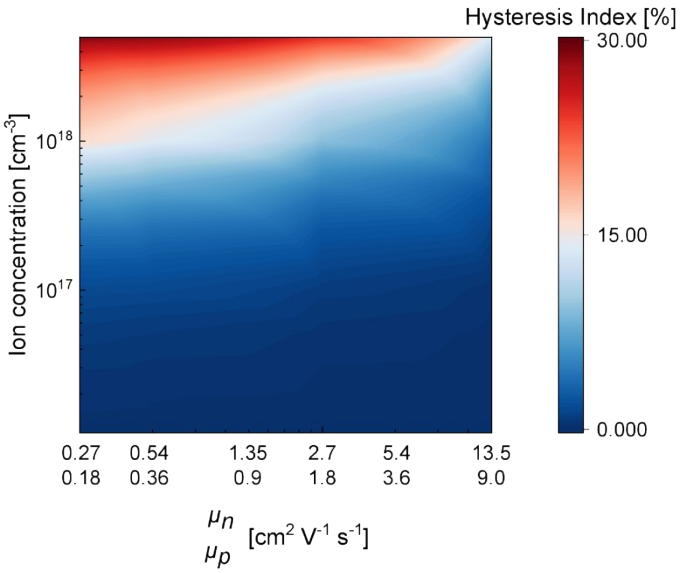

Supplementary Figure S7. HI contour maps for void devices under various carrier mobility and ion concentration.

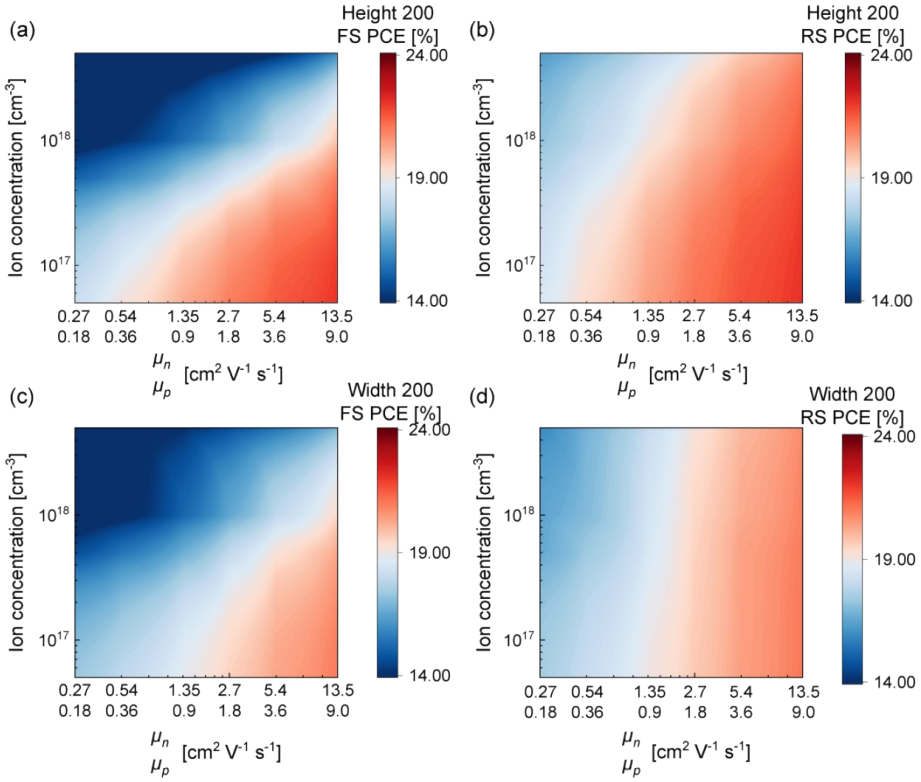

Supplementary Figure S8. PCE contour maps for device with relatively large (a-b) height or (c-d) width under forward and reverse voltage scans with various carrier mobility and ion concentration.

Table S1. Key parameters used in the simulation.

Parameter	Symbol	Unit	Perovskite	Spiro-OMeTAD	PCBM
Thickness	t	*nm*	400	150	40
GB width	*d*	*nm*	1	/	/
Permittivity	ε_r	/	6.6	3	3.9
Bandgap	E_g	*eV*	1.47	3	2
Electron affinity	E_a	*eV*	3.85	2.2	3.9
Effective DOS for electrons	N_C	cm^{-3}	1.2×10^{19}	1×10^{20}	1×10^{18}
Effective DOS for holes	N_V	cm^{-3}	2.9×10^{18}	1×10^{20}	2.4×10^{19}
Mobility of electrons	μ_n	$cm^2 V^{-1} s^{-1}$	2.7	2	0.2
Mobility of holes	μ_p	$cm^2 V^{-1} s^{-1}$	1.8	0.01	0.2
Doping concentration	N_A/N_D	cm^{-3}	1.3×10^{16}	1×10^{18}	1×10^{18}
Anion mobility	μ_a	$cm^2 V^{-1} s^{-1}$	1×10^{-12}	/	/

Parameter	Symbol	Unit	Perovskite	Spiro-OMeTAD	PCBM
Cation mobility	μ_c	$cm^2\ V^{-1}\ s^{-1}$	1×10^{-12}	/	/
Ion density	NI	cm^{-3}	5×10^{17}	/	/
Auger recombination coefficient	C_n/C_p	$cm^6\ s^{-1}$	1×10^{-28}	/	/
Direct recombination coefficient	C	$cm^3\ s^{-1}$	3×10^{-11}	/	/
Capture cross section	$\sigma_e/\sigma_{\mathrm{h}}$	cm^2	2×10^{-15}	/	/
Thermal velocity	$V_{th}^{e}/V_{th}^{\mathrm{h}}$	$cm\ s^{-1}$	1×10^{7}	/	/
Bulk trap density	N_t	cm^{-3}	5×10^{14}		
HTL/ETL interface density	N_t	cm^{-2}	1×10^{10}		
GB interface trap density	N_t	cm^{-2}	3×10^{11}		

Supplementary References

1. L. Shi, X. Liu, Y. Zhang, Y. Bao, T. Ma, L. Qin, G. Cao, C. Wang, C. Xiao, X. Li and Z. Yang, Multi-physics mechanisms and regulation of perovskite grain boundaries: insights into carrier dynamics, ion migration, thermodynamics, and thermal stress. *Energy Environ. Sci.*, **2025**, *18*, 7291-7301.
2. J. Liu, M. Adili, H. Pan, G. Hou, Y. Zhao, Q. Huang and X. Zhang, Simulation study on the impact of inorganic carrier transport layers on perovskite solar cell performance. *Sol. Energy*, **2025**, *288*, 113291.
3. R. Khan, N. Farjana, M.J.A. Jim, J.Y. Al-Humaidi, M.R. Islam and M.M. Rana, Numerical simulation and performance enhancement of CsBi3I10-based heterojunction solar cell with various semiconductor layers (CZTS, CZTGS, Al0. 8Ga0. 2Sb, GaAs) along with machine learning-based analysis. *Sol. Energy*, **2025**, *295*, 113539.
4. M.K.A. Mohammed, S.M. Abdalhadi, A. Kumar, O.P. Doshi, A.K. Al-Mousoi, H.T. Hussein, R.S. Alnayli, J. Madan, A.M. Tawfeek, M.F. Rahman and M.K. Hossain, Designing a novel hole-transporting layer for $FAPbI_3$-based perovskite solar cells. *Energy Fuels*, **2023**, *37*, 19870-19881.
5. K.I.F. Utsho, S.M.G. Mostafa, M. Tarekuzzaman, M.S.M. Al-Saleem, N.I. Nahid, J.Y. Al-Humaidi, M. Rasheduzzaman, M.M Rahman and M.Z. Hasan, Optimizing Cs 2 CuBiBr 6 double halide perovskite for solar applications: the role of electron transport layers in SCAPS-1D simulations. *RSC adv.*, **2025**, *15*, 2184-2204.
6. F.F. Targhi, Y.S. Jalili and F. Kanjouri, $MAPbI_3$ and $FAPbI_3$ perovskites as solar

cells: Case study on structural, electrical and optical properties. Results phys. **2018**, *10*, 616-627.

7. S.Z. Haider, H. Anwar and M. Wang, A comprehensive device modelling of perovskite solar cell with inorganic copper iodide as hole transport material. *Semicond. Sci. Technol.*, **2018**, *33*, 035001.

8. A.Hajjiah, M. Gamal, I. Kandas, N.E. Gorji and N. Shehata, DFT and AMPS-1D simulation analysis of all-perovskite solar cells based on $CsPbI_3$/$FAPbI_3$ bilayer structure. *Sol. Energy Mater. Sol. Cells,* **2022**, *248*, 112026.

9. H. Shen, D.A. Jacobs, Y. Wu, T. Duong, J. Peng, X. Wen, X. Fu, S.K. Karuturi, T.P. White, K. Weber and K.R. Catchpole, Inverted hysteresis in $CH_3NH_3PbI_3$ solar cells: role of stoichiometry and band alignment. *J. Phys. Chem. Lett.*, **2017**, *8*, 2672-2680.

10. S. Karthick, S. Velumani and J. Bouclé, Experimental and SCAPS simulated formamidinium perovskite solar cells: A comparison of device performance. *Sol. Energy*, **2020**, *205*, 349-357.

11.F. Ma, J. Li, W. Li, N. Lin, L. Wang and J. Qiao, Stable α/δ phase junction of formamidinium lead iodide perovskites for enhanced near-infrared emission. *Chem. Sci.*, **2017**, *8*, 800-805.